2.1. Simplification of RC building

The RC building is simplified to a SDOF model, as shown in Fig. 2. The equivalent height (H_{eq}), equivalent mass (M_{eq}), and equivalent stiffness (K_f) of the SDOF RC ($SDOF_{RC}$) model can be calculated by Eq. (1), Eq. (2) and Eq. (3), respectively, where m_i is the mass of i^{th} story, u_i is the displacement of i^{th} story, H_i is the height of i^{th} story, and T_f is the fundamental period of the first vibration mode.

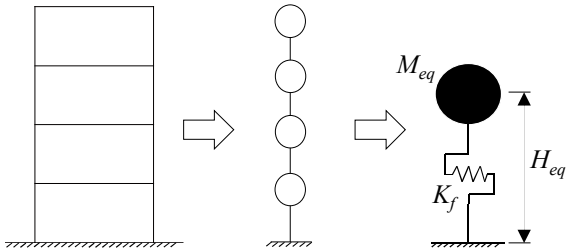

Existing RC building MDOF model Equivalent SDOF model

Fig. 2 – Simplification of the RC building to SDOF model

$$H_{eq} = \frac{\sum_{i=1}^{N} m_i \cdot u_i \cdot H_i}{\sum_{i=1}^{N} m_i \cdot u_i} \tag{1}$$

$$M_{eq} = \frac{\left(\sum_{i=1}^{N} m_i \cdot u_i\right)^2}{\sum_{i=1}^{N} m_i \cdot u_i^2} \tag{2}$$

$$K_f = \left(\frac{2\pi}{T_f}\right)^2 M_{eq} \tag{3}$$

Fig. 3 shows a simplified hysteretic response of $SDOF_{RC}$ at the pre-yielding (cracked, $\mu_c<\mu_f \leq 1$) and post yielding (yielding, $1<\mu_f$) stages [10]. The secant stiffness of the $SDOF_{RC}$ ($K_{f\mu}$) is pK_f, where p is the stiffness reduction coefficient determined from Eq. (4). Here, α_1 is pre-yield stiffness ratio, μ_c is the ratio of lateral crack (δ_{fc}) to lateral yield deformation (δ_{fy}), and μ_f is the ratio of the lateral target deformation (δ_{tar}) to δ_{fy}. E_f is hysteretic energy, and E_{fe} is the strain energy of the $SDOF_{RC}$. Q_{fc}, Q_{fy}, and Q_f are the lateral force at the crack, yield, and target deformation stages, respectively. The E_f is given in Eq. 5. The unloading stiffness (K_{ul}) is defined according to the Takeda degrading tri-linear model [15] for the cracked and yielding stages, where the unloading stiffness degradation parameter λ is assumed to be 0.4 [15].

$$\begin{aligned} p &= \frac{\mu_c + \alpha_1(\mu_f - \mu_c)}{\mu_f} && ;(\mu_c < \mu_f \leq 1) \\ p &= \frac{\mu_c + \alpha_1(1 - \mu_c)}{\mu_f} && ;(1 < \mu_f) \end{aligned} \tag{4}$$

$$\begin{aligned} E_f &= \frac{2K_f(\mu_f\delta_{fy})^2 \cdot (p \cdot (1-p) \cdot \mu_c)}{\mu_c + p\mu_f} && ;(\mu_c < \mu_f \leq 1) \\ E_f &= \frac{2pK_f(\mu_f\delta_{fy})^2 \cdot (p\mu_f - p(1-\mu_c)\mu_f^{\lambda} + \mu_c)}{\mu_c + p\mu_f} && ;(1 < \mu_f) \end{aligned} \tag{5}$$

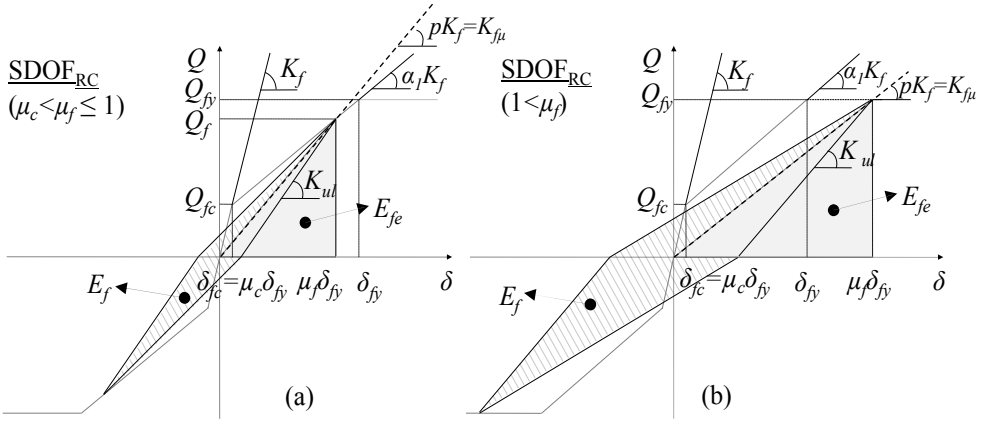

Fig. 3 –Hysteretic loops for $SDOF_{RC}$: (a) Cracked ($\mu_c < \mu_f \leq 1$) and (b) Yielding ($1 < \mu_f$)

2.2. Damper distribution to retrofitted RC building

This section presents the damper distribution to retrofit the RC building. The optimal equations to evaluate the required stiffness of EPD in the i^{th} story (K_{di}) and the required damping coefficient of FVD in the i^{th} story (C_{di}) are proposed in this section.

2.2.1. Elasto-plastic damper

The hysteretic response of EPD is considered on the SDOF system, which is parallel to the $SDOF_{RC}$. A simple elasto-perfectly plastic force-deformation relation is assumed for the EPD, while the supplemental SF is assumed to remain elastic through the design target story drift (θ_{tar}), as indicated in Fig. 4. The optimal equation to evaluate the parameters is the ratio of K_d/K_f, where the EPD stiffness (K_d) is assigned proportionally to the $SDOF_{RC}$ stiffness (K_f). The proposed equation is based on the following assumptions:

(a) The hysteretic energy of the EPD ($E_{d,EPD}$) is given in Eq. (6), where K_d is EPD stiffness, δ_{dy} is lateral yield deformation, and μ_d is damper ductility.

(b) The average equivalent hysteretic damping ratio for the retrofit system (h_{eq}) is assumed constant at all displacement amplitudes, and the h_{eq} can be estimated by Eq. (7), where the E_d is substituted by the $E_{d,\,EPD}$.

(c) The damping response reduction factor (D_h) was proposed in [14], as shown in Eq. (8). In this study, a=25 is used for real earthquake, where the inherent damping ratio of the $SDOF_{RC}$ (h_{f0}) is 3%, damping reduction factor (R) is 0.6 [10], To evaluate equivalent damping of $SDOF_{RC}$ ($h_{f\mu}$), E_d is substituted by zero.

(d) The target story drift at each story i^{th} ($\theta_{tar,i}$) is constant ($\theta_{tar,i} = \theta_{tar}$).

Therefore, the optimal ratio of the damper to frame stiffness (K_d/K_f) can be obtained by Eq. (9), where $\theta_{f\mu}$ is story drift of $SDOF_{RC}$, θ_{tar} is target story drift, $h_{f\mu}$ is the equivalent damping of $SDOF_{RC}$, μ_d is ductility factor of elasto-plastic damper, γ_s is stiffness ratio of steel frame to damper (this study assumes $\gamma_s = 0.05$).

$$E_{d,EPD} = 4K_d(\mu_d - 1)\left(\delta_{dy}\right)^2 \qquad ;(1 < \mu_d) \tag{6}$$

$$h_{eq} = h_{f0} + R\left(\frac{E_f + E_d}{4\pi E_{fe}}\right) \tag{7}$$

$$D_h = \sqrt{\frac{1 + ah_{f\mu}}{1 + ah_{eq}}} \tag{8}$$

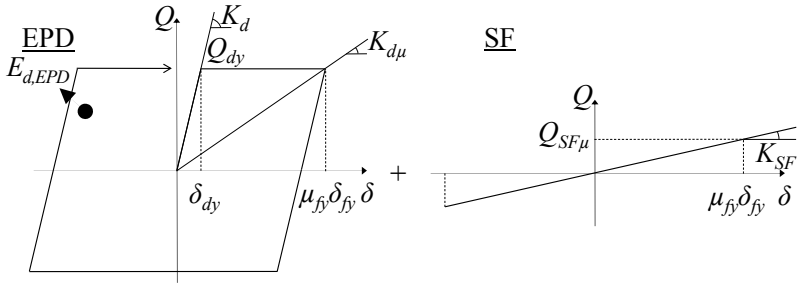

Fig. 4 –Hysteresis of EPD and SF

$$\frac{K_d}{K_f}=\frac{p\left(\frac{\theta_{f\mu}}{\theta_{tar}}\right)^2 D_h^2-p}{\gamma_s+\frac{1}{\mu_d}} \tag{9}$$

The K_{di}, as shown in Eq. (10), can be obtained with the following assumptions.

(a) The lateral force distribution along the building height for the i^{th} story (Q_i) can be calculated based on either A_i distribution described in the Japanese seismic design [16] or the ASCE-SEI7 specifications [17].

(b) Under the lateral force distribution, a maximum story drift (θ_{max}) at each story is equal to the θ_{tar}.

(c) The story damper (μ_{di}) and RC frame (μ_{fi}) ductilities at the θ_{max} are the same in all stories, as well as the steel frame-to-damper stiffness ratio (γ_{si}) are the same in all stories.

$$K_{di}=\frac{Q_i}{H_i}\frac{\sum_{i=1}^{N}\left(K_{f\mu i}H_i^2\right)}{\sum_{i=1}^{N}\left(Q_iH_i\right)}\left(\frac{1}{\gamma_s+\frac{1}{\mu_d}}+\frac{\mu_f}{\alpha_1(\mu_f-\mu_c)+\mu_c}\cdot\frac{K_d}{K_f}\right)-\frac{K_{f\mu i}}{\gamma_s+\frac{1}{\mu_d}} \quad ;(\mu_c<\mu_f\le 1)$$
$$K_{di}=\frac{Q_i}{H_i}\frac{\sum_{i=1}^{N}\left(K_{f\mu i}H_i^2\right)}{\sum_{i=1}^{N}\left(Q_iH_i\right)}\left(\frac{1}{\gamma_s+\frac{1}{\mu_d}}+\frac{\mu_f}{\alpha_1(1-\mu_c)+\mu_c}\cdot\frac{K_d}{K_f}\right)-\frac{K_{f\mu i}}{\gamma_s+\frac{1}{\mu_d}} \quad ;(1<\mu_f) \tag{10}$$

2.2.1. Fluid viscous damper

The concept of the proposed method is extended to FVD, which is a velocity-dependent device. Although the FVD does not have any inherent stiffness, this study assumes the viscous dampers are used serially attached to the elastic brace, which exhibits stiffness. Fig. 5(a) and Fig. 5(b) show the retrofitted model and retrofit configuration of the RC frame using FVD with SF. The viscous damper and additional SF force-deformation relationship are shown in Fig. 5(c). In this study, the viscous damper hysteretic response is considered as an equivalent SDOF system parallel to the $SDOF_{RC}$ and the SF. The hysteretic energy of the FVD ($E_{d,FVD}$) is given in Eq. (11), where K''_a is loss stiffness. The storage stiffness of the viscous damper (K'_a) can be calculated by Eq. (12), where K_b is the elastic brace stiffness, C_d is the damping coefficient of FVD, and ω is circular frequency. The ratio of the K''_a to K_f is introduced in Eq. (13), where η_a is the loss factor of the brace-damper subassembly in Eq. (14). The K''_a can be obtained by Eq. (15).

$$E_{d,FVD}=\pi K''_a\left(\mu_f\delta_{fy}\right)^2 \tag{11}$$

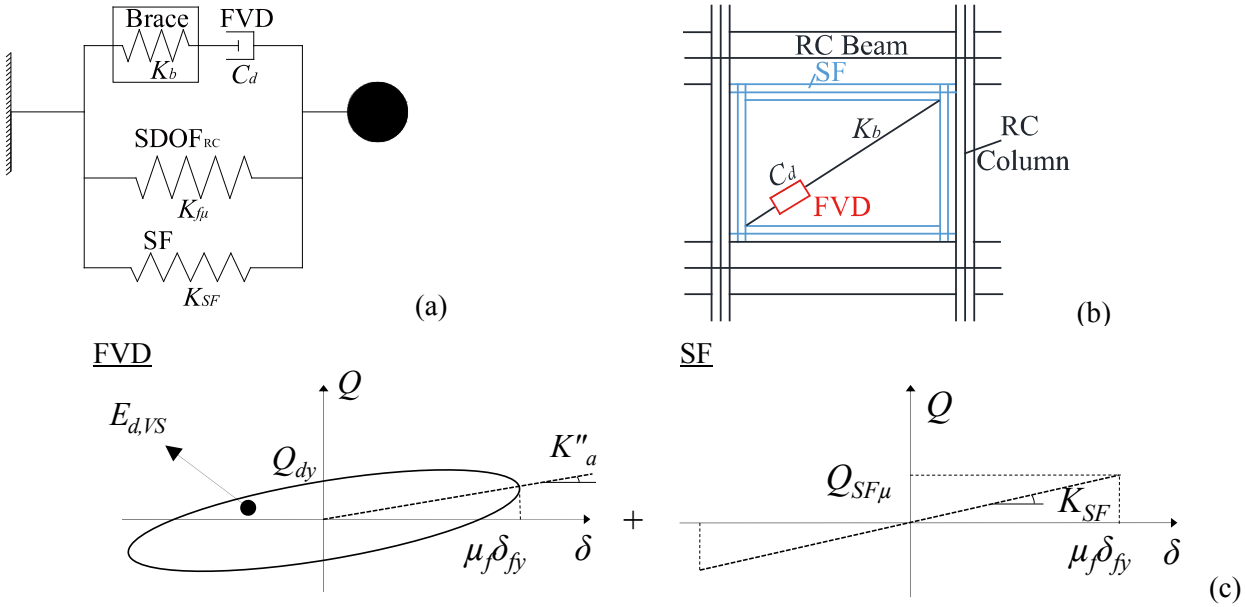

Fig. 5 –FVD (a) Retrofitted model, (b) Retrofit configuration, and (c) Hysteresis of FVD with a brace and SF

$$K'_a = \frac{C_d^2 K_b \omega^2}{K_b^2 + C_d^2 \omega^2} \tag{12}$$

$$\frac{K''_a}{K_f} = \frac{p\left(\frac{\theta_{f\mu}}{\theta_{tar}}\right)^2 D_h^2 - p}{\gamma_s + \frac{1}{\eta_a}} \tag{13}$$

$$\eta_a = \frac{K''_a}{K'_a} = \frac{K_b}{C_d \omega} \tag{14}$$

$$K''_a = \frac{C_d K_b^2 \omega}{K_b^2 + C_d^2 \omega^2} \tag{15}$$

The required loss stiffness of FVD (K''_{ai}) given in Eq. (16) can obtain with the following same assumptions as in the EPD case, where the η_a is assumed to be 1 for this study, and it is substituted in Eq. (15). Therefore, the required damping coefficient of FVD in the i^{th} story (C_{di}) can be obtained by Eq. (17).

$$K''_{ai} = \frac{Q_i}{H_i} \frac{\sum_{i=1}^{N}\left(K_{f\mu i} H_i^2\right)}{\sum_{i=1}^{N}\left(Q_i H_i\right)} \left(\frac{1}{\gamma_s + 1} + \frac{\mu_f}{\alpha_1(\mu_f - \mu_c) + \mu_c} \cdot \frac{K''_a}{K_f}\right) - \frac{K_{f\mu i}}{\gamma_s + 1} \qquad ;(\mu_c < \mu_f \le 1)$$

$$K''_{ai} = \frac{Q_i}{H_i} \frac{\sum_{i=1}^{N}\left(K_{f\mu i} H_i^2\right)}{\sum_{i=1}^{N}\left(Q_i H_i\right)} \left(\frac{1}{\gamma_s + 1} + \frac{\mu_f}{\alpha_1(1 - \mu_c) + \mu_c} \cdot \frac{K''_a}{K_f}\right) - \frac{K_{f\mu i}}{\gamma_s + 1} \qquad ;(1 < \mu_f) \tag{16}$$

$$C_{di} = \frac{2K''_{ai}}{\omega} \tag{17}$$

3. Target building and seismic region

A typical four-story RC school building is chosen as an example building in this study. The example RC building is located in Chiang Rai province, which is the northernmost province of Thailand. Fig. 6a and Fig. 6b show the elevation and structural plan of the four-story RC school building, respectively. Fig. 6c and Fig. 6d shows the cross-sectional member details of the RC beams and columns, respectively. The compressive strength of the concrete is 24 MPa, and the yield stress of the rebar is 300 MPa. The masses are 184 tons in the 1st to 3rd stories and 171 tons in the 4th story. The concrete slab is typically 100 mm thick in each story. Based on the modal analysis, the first to the third mode periods are 1.249 sec (translation in the longitudinal direction), 0.871 sec (torsional deformation), and 0.830 sec (translation in the transverse direction), respectively.

Fig. 7a and Fig. 7b present the design acceleration and displacement spectra, respectively, corresponding to a damping ratio of 5% in Thailand (Chiang Rai province) [18], where S_{DS} is the design spectral acceleration when the period is 0.2 sec and S_{D1} is the design spectral acceleration when the period is 1.0 sec. The target story drift ratio (θ_{tar}) is limited to 1/200 rad. (0.5% rad.).

The four-story RC school building is simplified to the $SDOF_{RC}$ model with the H_{eq} equals to 10 m (73.5% of building height), and the M_{eq} equals 577 tons (80% of the total mass). The lateral stiffness of the $SDOF_{RC}$ model in the longitudinal ($K_{f,l}$) and transverse ($K_{f,t}$) directions are 14.6 and 33.1 kN/mm, respectively. Based on the design displacement spectrum (Fig. 7b), the spectral displacements of the $SDOF_{RC}$ model are 76 and 48 mm in the longitudinal ($\delta_{d,l}$) and transverse ($\delta_{d,t}$) directions, respectively. The maximum story drift ratio (SDR_{max}) of the building in the longitudinal and transverse directions before retrofit is 0.76% ($=\delta_{d,l}/H_{eq}$) and 0.48% rad. ($\delta_{d,t}/H_{eq}$), respectively. Therefore, the retrofit is required only for the longitudinal direction. Fig. 6a also indicates retrofit location.

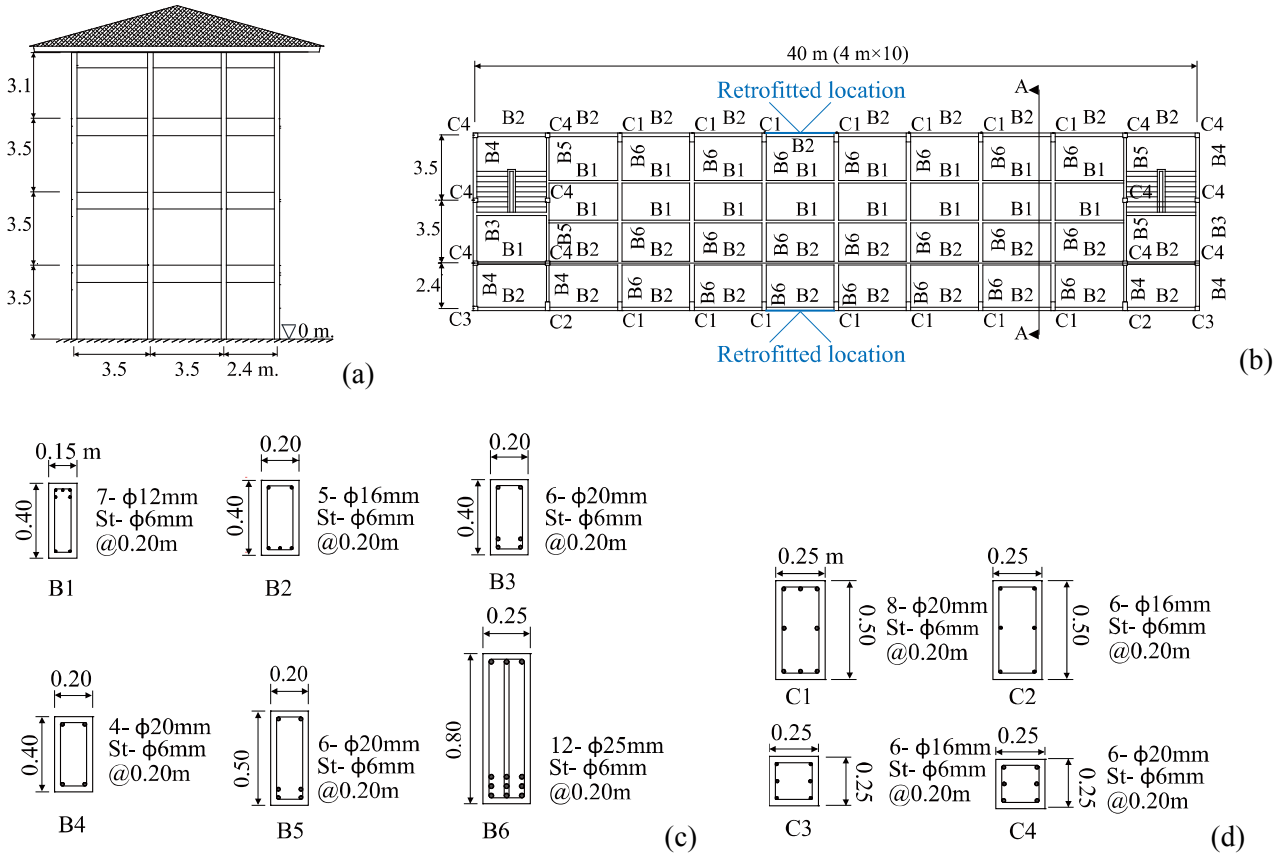

Fig. 6 –Details of the four-story RC school building (a) Section A-A, (b) Structural plan, (c) Cross-sectional details of the RC beams, and (d) Cross-sectional details of the RC columns

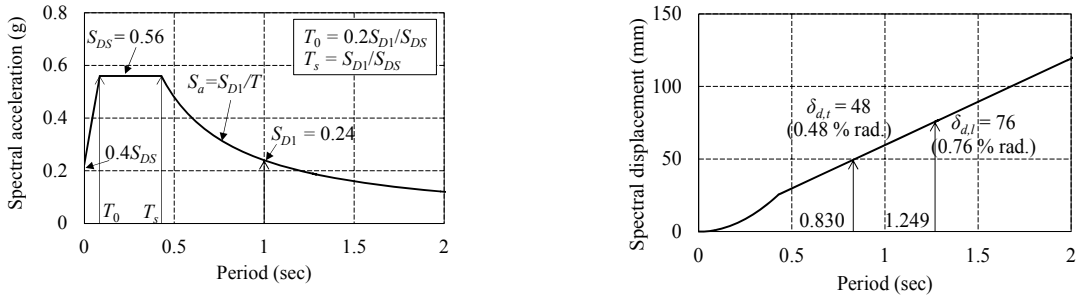

Fig. 7 –Design spectra of Chiang Rai province in Thailand (a) Acceleration and (b) Displacement.

4. Validation of the proposed retrofit design method

The proposed retrofit design method is examined on the target four-story RC school building. NLRHA is performed in order to validate the proposed retrofit method. Retrofit design examples of the four-story RC buildings using either EPD or FVD with SF is presented in this section. The details of ground motions, analysis models, and the analysis results are shown in the following.

4.1. Retrofit design example

Table 1 shows the retrofit design result of the example four-story RC school buildings using EPD with SF. The elastic stiffness of RC building in the i^{th} story (K_{fi}) is obtained by performing pushover analysis. The EPD to frame stiffness ratio (K_d/K_f) of 0.90 is calculated using Eq. (9). The required stiffness of EPD in the i^{th} story (K_{di}) is obtained by Eq. (10). Based on the proposed retrofit design method using EPD, the required EPD stiffness in the 4th (K_{d4}) is less than 0 under the design SDR_{tar} of 0.5%. Therefore, there is no need to install the EPD in the 4th story. This will be confirmed by the NLRHA results in the following sections.

Table 1. EPD distribution

Story	K_{fi} (kN/mm)	K_d/K_f	h_{eq}	K_{di} (kN)
4	39.6	0.90	0.064	-
3	32.2			34.8
2	32.1			65.4
1	45.3			43.7

Table 2 presents the retrofit design result of the example four-story RC school buildings using FVD with SF. The ratio of K''_a/K_f is obtained by Eq. (13), the K''_{ai} is calculated by Eq. (16), and the C_{di} is obtained by Eq. (17). Based on the proposed retrofit design method using FVD, the required loss stiffness of FVD in the 4th story (K''_{a4}) is less than 0, which is the same as the retrofitted RC building by using EPD under the design SDR_{tar} of 0.5%. Therefore, there is no need to install a FVD in the 4th story.

Table 2. FVD distribution

Story	K''_a/K_f	h_{eq}	ω (rad/s)	K''_a (kN/mm)	C_{di} (kN·sec/mm)
4	0.20	0.051	5.03	-	-
3				6.62	2.63
2				14.56	5.79
1				6.33	2.52

4.2. Analytical model

A three-dimensional (3-D) model was constructed using ETABS [19]. The model of the building without any retrofit (3D-R) is used as a benchmark model. Fig. 8 shows the 3-D model with retrofit using the EPD (3D-EPD). The model retrofitted with the FVD (3D-FVD) is constructed the same as the 3D-EPD apart from the

FVD is substituted instead of the EPD. It should be noted that the RC columns, RC beams, and slabs of all three models are the same. Based on Fig 7(b), the retrofit is required only for the longitudinal direction; therefore, the seismic response only in the longitudinal direction will be discussed in the following sections. The period of the 3-D model in the longitudinal direction of the 3D-FVD model is constant at 1.249 sec when compare the 3D-R model. The period decreases to 0.870 sec in the EPD model after the EPD has been installed.

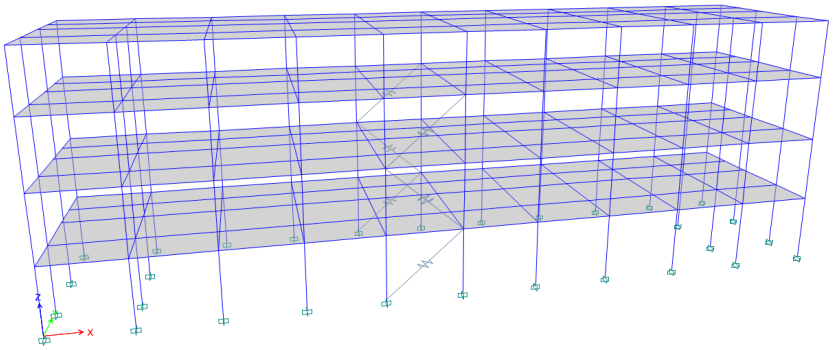

Fig. 8 –3-D view of the analytical model

4.3. Ground motions for NLRHA

A suite of scaled single component records is selected from the PEER NGA2 ground motion database 2 [20]. The detail of each ground motion is shown in Table 3, and the scaled spectra are shown in Fig. 9. The scaling is conducted over a target period range of $0.2T_1$ and $1.5T_1$, where T_1 is the fundamental period of the non-retrofitted building. The scaling follows the requirements described in [17].

Table 3 Ground motions used for NLRHA

Ground ID (GM)	Earthquake Name	Year	Station Name	Magnitude	Scaling factor
1	Imperial Valley-06	1979	El Centro Array #13	6.5	1.89
2	Kobe_Japan	1995	Sakai	6.9	1.32
3	El Mayor-Cucapah	2010	Holtville Post	7.2	1.20

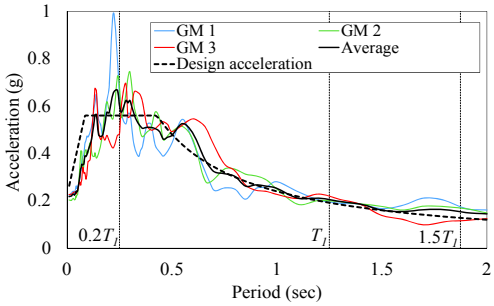

Fig. 9 – 5% damped response spectra of the scaled ground motions and the design acceleration spectrum.

4.4. NLRHA result

The NLRHA is performed on the 3D-R, 3D-EPD, and 3D-FVD models using three scaled ground motions to investigate the seismic response and validate the proposed retrofit method. The results of each ground and average from the NLRHA are shown in the following.

4.4.1. Maximum story drift ratio

The maximum story drift ratio (SDR_{max}) responses of each ground motion for the 3D-R, 3D-EPD, and 3D-FVD models are shown in Figs 10(a), 10(b), and 10(c), respectively. Fig 10(a) shows the SDR_{max} of the RC building without retrofit (3D-R) model. The SDR_{max} in 1st to 3rd stories, as obtained from NLRHA with all ground motions, exceed the SDR_{tar} of 0.5% rad. These results agree with the proposed retrofit method that no damper is required in the 4th story, as shown in Table 1, for the case of installing EPD and Table 2 for the case of installing FVD. Fig 10(b) and Fig 10(c) present the SDR_{max} of the 3D-EPD and 3D-FVD, respectively. The analysis results of all ground motions indicate that the proposed retrofit method using either EPD or FVD with SF can efficiently limit the SDR_{max} in every story within SDR_{tar} of 0.5% rad. The SDR_{max} is uniform after retrofit using both types of dampers with SF. The SDR_{max} of all stories except the 4th story is in line with the SDR_{tar} of 0.5% rad. It implies that the proposed retrofit method using either EPD or FVD with SF can result in SDR_{max} close to the SDR_{tar}.

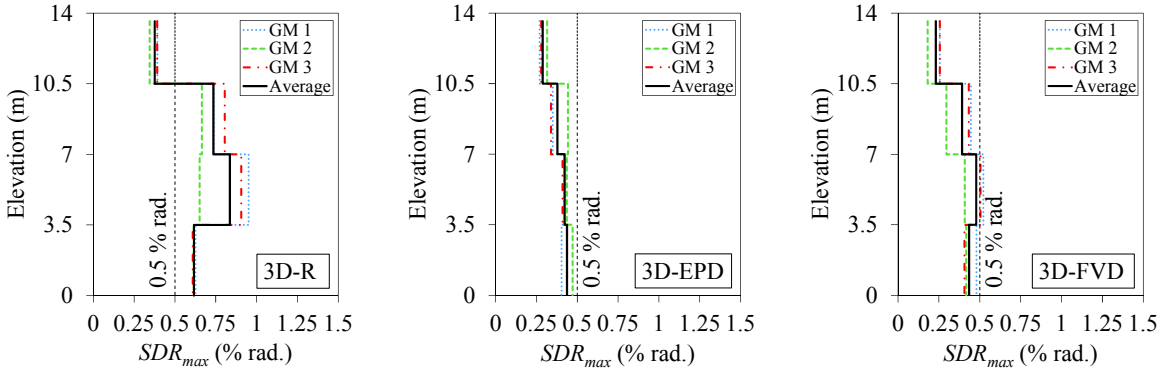

Fig. 10 –Maximum story drift ratio

4.4.2. Residual story drift ratio

The residual drift ratio (SDR_{re}) responses of each ground motion for the 3D-R, 3D-EPD, and 3D-FVD models are shown in Figs 11(a), 11(b), and 11(c), respectively. Figs 11(a) shows SDR_{re} of the RC building without retrofit. The analysis result of the bare RC building indicates that the SDR_{re} exceeds 0.1% for the 1st, 2nd, and 3rd stories, and the distribution of SDR_{re} along the building height is not uniform. Figs 11(b) and 11(c) present the SDR_{re} of 3D-EPD and 3D-FVD models, respectively. The results of all ground motions for both 3D-EPD and 3D-FVD models indicate that the SDR_{re} is reduced significantly, and the SDR_{re} is much smaller than 0.1% after retrofitted RC building using either EPD or FVD with SF. It implies that both structural and non-structural damage can be mitigated for the retrofitted buildings.

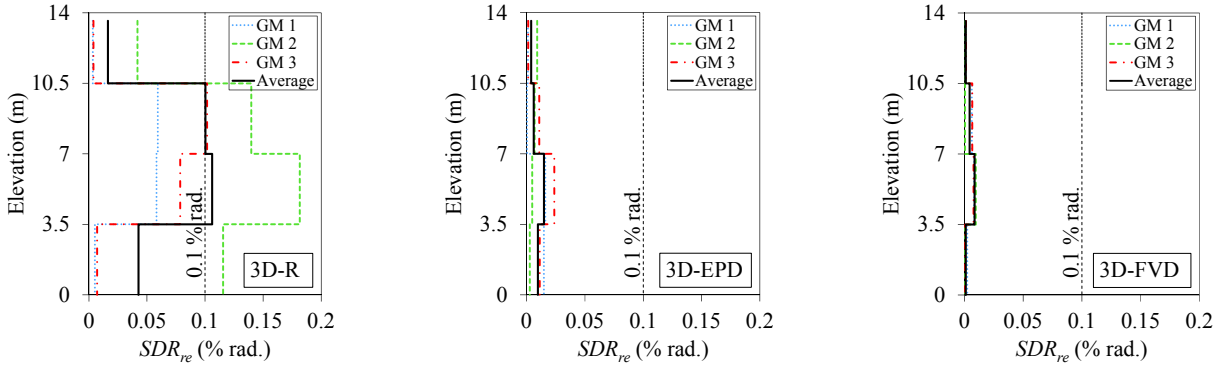

Fig. 11 –Residual story drift ratio

4.4.3. Maximum acceleration

Figs 12 shows the maximum acceleration (A_{max}) responses of the 3D-R, 3D-EPD, and 3D-EPD models as obtained from the NLRHA. The trend of the A_{max} is decreased for the retrofitted buildings by both EPD and FVD. Based on the NLRHA analysis, the A_{max} of the retrofitted RC building with FVD significantly reduces by around 29 % to 44 % when compared to the bare RC building without retrofit. For the retrofitted with EPD, the A_{max} decreases by about 10% when compared to the bare RC building without retrofit. The reduction in the A_{max} value of the retrofitted with dampers is expected because the SDR_{max} can be efficiently limited by using dampers, and the energy-dissipated by the dampers can increase the total damping of the retrofitted buildings.

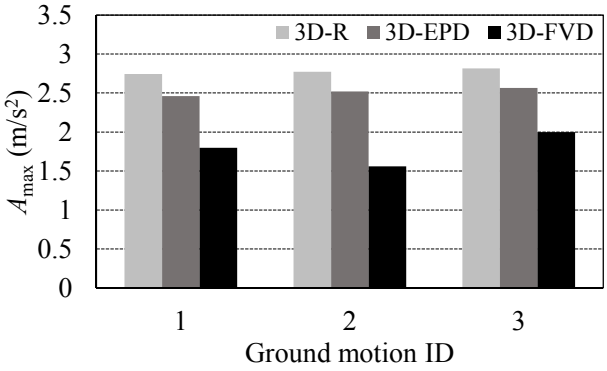

Fig. 12 –Maximum roof acceleration

5. Conclusions

The seismic retrofit method of RC building using either EPD or FVD implementing SF based on equivalent linearization without an iterative procedure to achieve the design SDR_{tar} is introduced. The proposed method is validated by NLRHA on the four-story RC school building. The response of the existing bare RC building was compared to retrofitted RC buildings using dampers with SF. The conclusions of this study can be drawn as follows:

1) The installation of either EPD or FVD to the bare RC building can improve the seismic performance of the RC building. The SDR_{max} of the retrofitted building can be reduced significantly.

2) Based on the example retrofit design, the SDR_{max} in the 1st to the 3rd stories as obtained from NLRHA with all ground motions exceed the SDR_{tar}. However, the SDR_{max} in the 4th was within the SDR_{tar}. This agrees with the proposed retrofit evaluation that no retrofitted damper is required in the 4th story.

3) The NLRHA analysis result suggests that the proposed retrofit method can result in the SDR_{max} close to the design SDR_{tar}. The SDR_{max} values were controlled within the SDR_{tar} in all stories when both types of dampers retrofitted the RC building.

4) The SDR_{re} of the retrofitted RC building using either EPD or FVD implementing SF can be controlled within 0.1%, which implied that both structural and non-structural damage could be mitigated in the retrofitted buildings.

5). Based on the example retrofit design, the trend of A_{max} was decreased after the building was retrofitted. The reduction in the A_{max} value can be expected because the SDR_{max} can be efficiently limited by using both types of the damper, and the energy-dissipated by the dampers can increase the total damping of the retrofitted buildings. The A_{max} is significantly reduced by 29% to 44% for the building retrofitted with FVD, and the reduction of A_{max} is reduced by 10% for retrofitted RC building with EPD.

6. References

[1] Martinez-Rodrigo M., Romero M.L (2003): An optimum retrofit strategy for moment resisting frames with nonlinear viscous dampers for seismic applications. *Engineering Structures*, **25**, 913-925.

[2] Jinkoo Kim, Choi H. (2006): Displacement-based design of supplemental dampers for seismic retrofit of a framed structure *Journal of Structural Engineering*, **132**, 873-883.

[3] Chang K.C., Lin Y.Y., Chen C.Y. (2008): Shaking table study on displacement-based design for seismic retrofit of existing buildings using nonlinear viscous dampers. *Journal of Structural Engineering*, **134**, 671-681.

[4] Kunisue A, Koshika N, Kurokawa Y, Suzuki N, Agami J, Sakamoto M (2000): Retrofitting method of existing reinforced concrete buildings using elasto-plastic steel dampers. *12th World Conference of Earthquake Engineering*.

[5] Fujimoto M, Wada A, Saeki E, Takeuchi T, Watanabe A (1990): Development of unbonded brace. *Quarterly Column*, **115**, 91-96.

[6] Sarno L.D, Manfredi G. (2012): Experimental tests on full-scale RC unretrofitted frame and retrofitted with buckling-restrained braces. *Engineering & Structural Dynamics*, **41**, 315-333.

[7] Takeuchi T, Yasuda K, Iwata M. (2009): Seismic retrofitting using energy dissipation façade. *ATC-SEI09 Conference on Improving the Seismic Performance of Buildings and Other Structures*.

[8] Mahrenholtz1 C, Lin P.C, Wu A.C, Tsai K.C, Hwang S.J.H, Lin R.Y, Bhayusukma M.Y. (2015): Retrofit of reinforced concrete frames with buckling-restrained braces. *Engineering & Structural Dynamics*, **44**, 59–78.

[9] Khampanit A, Leelataviwat A, Kochanin J, Warnitchai P. (2014): Energy-based seismic strengthening design of non-ductile reinforced concrete frames using buckling-restrained braces. *Engineering Structures*, **81**, 110-122.

[10] Sutcu F, Takeuchi T, Matsui R. (2014): Seismic retrofitting design method of existing RC buildings with buckling restrained braces, *Journal of Constructional Steel Research*, **101**, 304–313.

[11] Sutcu F, Bal A, Fujishita K, Celik O. C, Takeuchi T, Matsui R, Terashima M, Maeda Y (2017): Near full-scale experimental investigation of low-standard RC frames retrofitted with buckling-restrained braces. *16th World Conference of Earthquake Engineering*.

[12] D. LEE, Taylor D.P. (2001): Viscous damper development and future trends. *Struct. Design Tall Build*. **10**, 311-320

[13] Fujishita K, Sutcu F, Matsui R, Takeuchi T. (2005): Damage distribution based energy-dissipation retrofit method for multi-story RC building in Turkey. *IABSE Symposium Report*, **104**, 1–8.

[14] Kasai K, Fu Y, Watanabe A (1998): Passive control systems for seismic damage mitigation. *Journal of Structural Engineering*, **124**, 501-512.

[15] Takeda T, Sozen M.A, Nielsen N.N (1970): Reinforced concrete response to simulated earthquakes. *Journal of Structural Engineering*, **96**; 2557-2573.

[16] The Building Center of Japan. The Building Standard Law of Japan on CD-ROM 2016.

[17] American Society of Civil Engineers (ASCE) (2016): Minimum Design Loads for Buildings and Other Structures 2016 (ASCE/SEI 7-16).

[18] Department of Public Works and Town & Country Planning (DPT) (2009): Thailand Seismic Design Code.

[19] Wilson E.L (2015): CSI analysis reference manual for SAP 2000 ETABS, SAFE, and CSI Bridge. Berkeley, Computers & Structures, Inc 2015.

[20] Pacific Earthquake Engineering Research Center (PEER). PEER NGA Ground motion database, < http://ngawest2.berkeley.edu/site >

